Blind Identification Algorithm Of Photorealistic Computer Grapic Based On Weber Local Features

Liu Xicheng, Xi Jianzhong
School of Electrical Engineering and Informationy Southwest Petroleum University, Chengdu, Sichuan, 610500, China
liuxicheng036@163.com

Journal of Digital Information Management

ABSTRACT: *Digital image tampering technology having developed with the emergence of the information age, computer software can be used to draw a variety of scene images whose authenticity is undistinguishable to human naked eyes. On account of the challenges to image authenticity, this paper introduces digital image forensics technology. Based on the imaging mechanism and differences of photographic images (PIM) and photorealistic computer graphics (PRCG), images were transformed from red, green and blue (RGB) color space to hue, saturation and value (HSV) color space with PRCG blind identification technology. Then, Weber local features of single-channel image of HSV color space were extracted, including the histogram features of differential excitation information, Sobel gradient direction information and Sobel gradient magnitude information. At last, all the classification features were trained and tested in support vector machine (SVM) classifiers. The experimental results indicate that the algorithm can effectively reduce the dimensionality of the features and increase the detection rate.*

Subject Categories and Descriptors
I.4.1 [Digitization and Image Capture]; I.4.8 [Scene Analysis]: Photometry

General Terms: High Performance System, Parallel Technologies

Keywords: Photographic images, Image tampering technology, Weber local feature, Blind identification of images

Received: 26 January 2016, Revised 2 March 2016, Accepted 11 March 2016

1. Introduction

Contemporarily, digital cameras and printers have been upgraded constantly, and the traditional film images have gradually been replaced by digital images. With the development of digital image technology, digital image processing software technology is in constant innovation and development. For instance, digital image forensics technology has been developed to judge whether images are authentic, complete and original [1, 2], involving multiple disciplines such as computer graphics, image processing, computer vision, machine learning and information security [3]. Based on whether information preprocessing is necessary, digital image forensics technology is divided into active digital image forensics (based on digital watermarking or digital signature) and passive digital image forensics [4-6].

Different from active digital image forensics technology, passive digital image forensics does not involve image preprocessing; instead, authenticity and source of the images can be identified based on characteristics of the images, thus passive digital image forensics is also known as blind digital image forensics technology [7] which can be divided into two categories of blind image forensics technologies oriented by authenticity detection or identification of the sources [8]. Compared with active digital image forensics technology, digital image blind blind forensics technology is advantageous in sparing

preprocessing such as digital signature or embedding digital watermarking.

The blind identification algorithms for photographic images (PIM) and photorealistic computer graphics (PRCG) are divided into two categories based on the differences in statistical characteristics or imaging process [9]. The two kinds of algorithms applied machine learning method, namely, the algorithm was regarded as a dichotomy problem of photographic images and computer generated images [10]. At present, both in China and other countries, researches on blind identification algorithms are mostly based on extracting the statistical features of images, such as wavelet high order statistical features, fractal dimension features, coherence of adjacent pixels, characteristics of local energy variance, features of histogram frequency domain moments, second order difference statistic features, image quality assessment features and statistical features of photographic images [11]. Then, the extracted classification features are trained and tested in support vector machine (SVM) classifiers. On account of the convenience for use and extensive application of blind identification technology of images, this study is performed with regard to blind identification method of images from the aspect of local image features.

2. Blind Identification Algorithm of Computer Generated Images Based on Weber Local Features

Based on Weber's law, Weber local feature is proposed as a kind of local feature that can describe the local detail variations of images, including two components (differential excitation and direction information) which can be unified by means of two-dimension joint histogram [12].

2.1 Weber's law

Discovered by a German physiologist Weber, Weber's law is used to represent the relationship between physical quantity and psychological quantity [13]. Weber found that only when the ratio of incentive variation quantity and the original incentive quantity was greater than or equal to a constant, can the variation be perceived. The law can be described by the following formula.

$$k=\frac{\Delta I}{I} \qquad (1)$$

In formula (1), *k* refers to Weber ratio; "*I* refers to stimulus variation; *I* refers to the original stimulation. According to Weber's law, two different ratios are used to describe the texture changes in images, differential excitation and orientation information can be obtained and combined, thus a two-dimensional histogram feature is obtained.

2.2 Differential excitation

Differential excitation component is calculated according to a ratio of which the numerator is the sum of the differences between gray values of the current pixel and its neighborhood pixels, while the denominator is the current pixel itself [14-16]. The concrete steps are as follows:

Firstly, filter windows f1 and f2 are used for filtering processing on the input images, and the first ratio matrix G1 is obtained:

$$v_1=I*f_1, v_2=I*f_2, G_1=\frac{v_1}{v_2} \qquad (2)$$

In formula (2), * denotes convolution operation; *I* refers to the input image. As is shown in Figure 1, *f1* refers to Laplace filter; *v1* refers to the change of gray level of the filtered image; *f2* refers to the filtering result; *v2* refers to the input image. The scope of the ratio matrix *G1* is $[-\infty,+\infty]$. According to formula (3), *G1* can be mapped to

$$\alpha\in\left[-\frac{\pi}{2},\frac{\pi}{2}\right]$$

$$\alpha=\arctan(G_1)=\arctan(\frac{v_1}{v_2}) \qquad (3)$$

Finally, each value in matrix α is linearly quantized to *L1* level. Then, if the values in matrix α are within the range of $\left[-\frac{\pi}{2}+\frac{(i-1)\pi}{L_1},-\frac{\pi}{2}+\frac{i\pi}{L_1}\right)$, they will be quantified into a constant ξ_i. In order to facilitate the establishment of statistical histogram, we suppose $\xi_i = i$. According to formula (4), the quantified differential excitation matrix *E* can be calculated

$$E=\{\xi_i\}=\left[\frac{\alpha+\frac{\pi}{2}}{\frac{\pi}{L_1}}\right], i=1,2,\cdots,L_1 \qquad (4)$$

1	1	1
1	-8	1
1	1	1

f_1

0	0	0
0	1	0
0	0	0

f_2

1	2	1
0	0	0
-1	-2	-1

f_3

1	0	-1
2	0	-2
1	0	-1

f_4

Figure 1. Filtering windows in Weber's local features

2.3 Direction information

Directional information component refers to solving the gradient directions of images according to the ratio of gray level changes in vertical direction and horizontal direction [17, 18]. The specific steps are as follows.

Firstly, filtering windows *f3* and *f4* are used for filtering processing on the input images, and the second ratio matrix *G2* can be calculated:

$$v_3 = I * f_3, v_4 = I * f_4, \ G_2 = \frac{v_3}{v_4} \qquad (5)$$

As shown in Figure 1, *f3* and *f4* are Sobel operators; their filtering results are *v3* and *v4*; respectively, *v3* represents the change of images in vertical direction, while *v4* represents the change of images in horizontal direction. The range of *G2* is $[-\infty, +\infty]$. According to formula (6), the ratio matrix *G2* is mapped to $\theta \in \left[-\frac{\pi}{2}, \frac{\pi}{2}\right]$:

$$\theta = \arctan(G_2) = \arctan\left(\frac{v_3}{v_4}\right) \qquad (6)$$

Then, according to the positive and negative conditions of *v3* and *v4*, ¸ is transformed to $\theta' \in [0, 2\pi]$.

$$\theta'(x,y) = \begin{cases} \theta(x,y), & v_3(x,y)>0, \ v_4(x,y)>0 \\ \theta(x,y)+\pi, & v_3(x,y)<0, \ v_4(x,y)>0 \\ \theta(x,y)+\pi, & v_3(x,y)<0, \ v_4(x,y)<0 \\ \theta(x,y)+2\pi, & v_3(x,y)>0, \ v_4(x,y)<0 \end{cases} \qquad (7)$$

In formula (7), (*x*, *y*) represents a coordinate in the matrix; the gradient direction matrix θ' is further linearly quantized to L_2 level. Accordingly, in the gradient direction matrix θ', the values within the range of are quantified into a constant ψ_j. Similarly, suppose ψ_j=1, then, according to formula (8), the quantified gradient direction matrix *O* can be obtained.

2.4 Weber local histogram

Two-dimensional histogram statistics can be obtained by combining the differential excitation and direction information. The calculation steps are as follows.

$$WLD(i,j) = \frac{\sum \delta_{ij}(x,y)}{XY}, i=1,2,\cdots,L_1; j=1,2,\cdots,L_2 \qquad (9)$$

$$\sigma_{ij}(x,y) = \begin{cases} 1, E(x,y)=\xi i, O(x,y)=\psi_j \\ 0, \quad others \end{cases} \qquad (10)$$

In formula (9), *X* and *Y* respectively denote the line number and column number of image matrix *I*; (*x*, *y*) refers to the coordinate in matrix; *WLD* (*i*, *j*) refers to the value at line *i*, column *j* in 2D Weber local histogram. As shown in Figure 2, the two-dimensional Weber local histogram is transformed into a one-dimensional histogram vector. First, sub-histograms of each line are extracted from the two-dimensional Weber local histogram; then, all the sub-histograms are integrated into a one-dimensional histogram feature vector h whose length is L1 × L2.

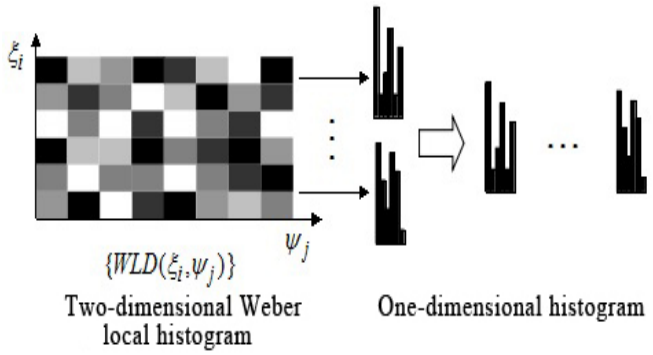

Figure 2. Weber local histogram

3. Algorithm Process

3.1 The basic process

Firstly, the image library was divided into two parts— training images and test images. Then, the images were transformed from RGB color space to HSV color space. After color channel separation, three single-channel images (H, S and V) were obtained. According to training images, feature vectors were constructed for the establishment of classified models. Based on the given calculation method of Weber local descriptor (WLD) features, WLD histogram features of single-channel images of training images were extracted; then, with SVM classifier, training was performed and classified models were built. At last, classified models were used for image testing. As to the testing images, extraction and construction of feature vectors were performed in the same manner; the obtained classified models were used for testing, thus the classification results were obtained.

3.2 HSV color space

HSV color space is similar to RGB color space. The color parameter of the model consists of hue, saturation and value. The three-dimensional sketch map is shown in Figure 3.

H refers to hue, and 0 < *H* < 360; if *H* < 0, *H* = *H* + 360. S refers to saturation, and 0 < S < 1.

Brightness and color information (hue and saturation) were separated so that the color space was corresponding to human visual perception, better reflecting human identification of colors [19-21]. To sum up, compared with RGB color space, HSV color space was more suitable for the identification of photographic images and photorealistic computer graphics. Therefore, this study identified the images by extracting WLD features of HSV color space.

The algorithm of transforming RGB into HSV is shown in formula (11). Max refers to the maximum values of thethe three colors RGB of pixel points, while min refers to the minimum values of the three colors RGB of pixel points. According to formula (11), the values of H, S and V were solved.

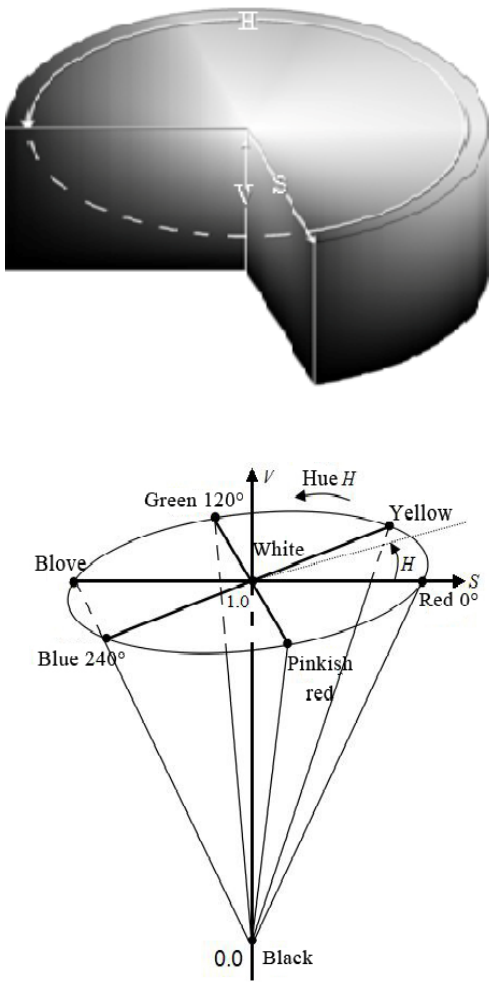

Figure 3. Three-dimensional sketch map of HSV color space

$$H=60^{*}\begin{cases}\frac{G-B}{\max-\min} & if\ \max=R\\ \frac{B-R}{\max-\min}+2 & if\ \max=G\\ \frac{R-G}{\max-\min}+4 & if\ \max=B\\ not\ defined\end{cases}$$

$$S=\begin{cases}\frac{\max-\min}{\max} & if\ \mathrm{Max}\neq 0\\ 0 & if\ \mathrm{Max}=0\end{cases}$$

$$V=\max(R,G,B) \qquad (11)$$

colored image by color transforming. Then, WLD features of the single-channel image of HSV color space were extracted. The detailed procedures are as follows.

Taking H channel as an example, its WLD features were extracted. Respectively, differential excitation and Sobel gradient direction information were quantified into *k1* and *k2* level; then, they were stored in the matrix. And then, three matrixes in consistent size with the image were obtained, respectively used for the storage of quantification information of differential excitation, Sobel gradient direction and Sobel gradient magnitude.

The histograms of the above three matrixes were calculated. As to the histogram obtained from Sobel gradient information matrix, considering that the proportion of subsequent deviation values was approximate to 0, we only selected the components whose values were the first *k3* deviation values. Thus we obtained the (*k1* + *k2* + *k3*) dimensional classified features of the first group.

As to the images of S channel and V channel, repeating the procedures above, we obtained (*k1* + *k2* + *k3*) × 3 dimensional features.

4. Experimental Results and Analysis

4.1 Image library

The image library adopted in this study contained 1500 photographic images and 1250 photorealistic computer graphics (the sample images are shown in Figure 4 and Figure 5) which were used to test classification performance of the classification features. Resolution ratios of the images were varied, such as 737×492 and 722×480; the storage format was JPEG. For each experiment, 1200 photographic images and 1000 photorealistic computer graphics were randomly selected as training samples from the image library, while the remaining images were used as testing samples. On account that the random selection of samples might affect the experimental results to some degree, we selected the average values of 10 experimental results to evaluate the classification performance of the classification features.

This study adopted receiver operating characteristics (ROC) curve and detection rate to evaluate performance of the algorithm. The larger the area under ROC was, the better the classification performance would be [22]. The detection rate included the true positive (TP) detection rate of photorealistic computer graphics, true negative detection rate of photographic images and the overall detection rate (accuracy). The evaluation index was defined as: TP = amount of correctly classified PRCG samples / amount of the samples regarded as PRCG; TN = amount of correctly classified PIM samples / amount of the samples regarded as PIM; accuracy = total amount of correctly classified PRCG and PIM samples / total amount of samples.

4.2 Experimental procedures

(1) The target color image was input and its attribute label (1 for photographic images and -1 for photorealistic computer graphics) was obtained.

(2) The image was transformed from RGB color space into HSV color space and separated to obtain three single-channel images (H, S and V).

Figure 4. Photographic images

Figure 5. Photorealistic computer graphics

(3) Respectively, WLD histogram features of the three single-channel images (H, S and V) were extracted, including the information of differential excitation, Sobel gradient direction and gradient magnitude.

(4) Training was performed with an SVM classifier; grid search method was used to automatically search the optimal punishment factor C and parameter ^{3} of kernel function, and the classified model was established.

(5) The established classified model was used to detect the testing image, then, its TP, TN and Accuracy were obtained.

4.3 Receiver operating characteristics curve

Figure 3.6 shows the ROC curve which measures the predicting results of the above testing sample images. S refers to the area that ROC curve and the below coordinate axis formed. The greater the value of S was, the more accurate the prediction was. As can be seen from Figure 6, AUC in the experiment was up to 0.9458 which was a relatively ideal value, compared with the optimal prediction result of 1. According to Table 4, the accuracy of the algorithm was up to 95.79% in detecting photographic images and 94.98% in detecting photorealistic computer graphics. Accordingly, the overall detection accuracy was 95.43%.

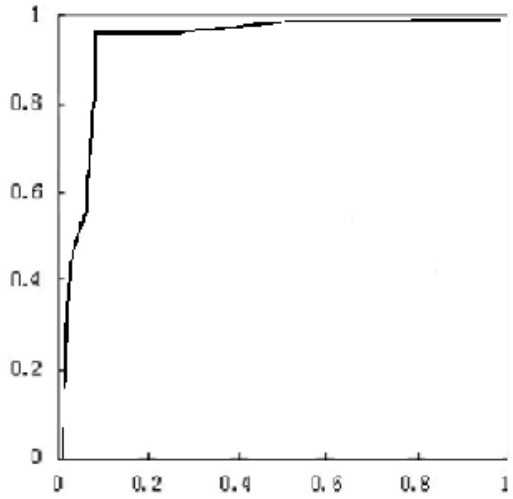

Figure 6. ROC curve (the horizontal ordinate represents specificity; the vertical ordinate represents sensitivity)

4.4 Parameter settings

Based on experiments, this study selected the specific feature dimensions of the three histogram feature components from the improved WLD features. The specific dimensions are as follows.

4.4.1 Histogram feature dimension *k1* of differential excitation information

k_1	*TP(%)*	*TN(%)*	*Accuracy(%)*
1	55.00	80.04	68.02
2	79.00	89.36	84.98
3	74.00	88.15	81.12
4	77.00	87.52	82.03
5	36.00	90.61	69.81
6	79.00	89.36	84.98
7	82.00	81.26	82.04
8	79.00	89.36	84.98
9	79.00	89.36	84.98
10	82.00	81.26	82.04

Table 1. Experimental results of feature dimensions of differential excitation information

Table 1 shows the relationship between the classification performance and histogram feature dimensions of differential excitation information. When the values of *k1* ranged from 1 to 5, the detection performance (either detection rate of photographic images or detection rate of photorealistic computer graphics) was in a gradual increasing trend. When the values of *k1* ranged from 5 to 8, all the detection rates were in a stable condition. When the values of *k1* ranged from 8 to 10, detection rate of photorealistic computer graphics increased to some extent; however, the detection rate of photographic images and the overall detection rate declined. With overall consideration on feature dimensions and detection performance, we determined the value of *k1* to be 5.

4.4.2 Histogram feature dimension *k2* of Sobel gradient direction information

Table 2 shows the relationship between the classification performance and histogram feature dimensions of Sobel gradient direction information. The detection performance of photorealistic computer graphics increased first and then decreased with the increasing values of *k2*, while the detection rate of photographic images first decreased and then increased. However, according to the experimental results, values of feature components in feature vectors tended to be 0, and the classification performance reached its peak when the value of *k2* was 9. Considering the detection rate and feature dimension, the value of *k2* was determined to be 9.

k_2	TP (%)	TN (%)	Accuracy (%)
1	58.00	80.02	71.91
2	74.00	80.62	77.71
3	65.00	80.02	74.63
4	56.00	80.02	71.18
5	38.00	85.64	67.33
6	70.00	74.99	73.05
7	78.00	83.74	81.55
8	75.00	81.26	78.86
9	71.00	82.48	78.10
10	82.00	81.85	81.92

Table 2. Experimental results of the feature dimension of Sobel gradient direction information

4.4.3 Histogram feature dimension of Sobel gradient magnitude information

Table 3 shows the relationship between classification performance and histogram feature dimension of Sobel gradient magnitude information. The detection performance of both photographic images and photorealistic computer graphics first increased and then decreased with the increasing values of *k3*, which might be because the values of subsequent feature components were close to 0 while the values of *k3* were increasing. The value of *k3* was determined to be 6 when the detection rate was the highest.

In summary, in order to ensure the detection rate and reduce feature dimensions, we determ989ined *k1* = 5, *k2* = 9, *k3* = 6. Accordingly, we obtained (5+9+6) × 3 = 60 dimensional features which were used as classification features to detect photographic images and photorealistic computer graphics.

*k*3	TP(%)	TN (%)	Accuracy (%)
1	58.00	88.76	76.90
2	68.00	93.76	83.86
3	62.00	91.86	79.38
4	65.00	94.35	83.09
5	31.00	96.24	71.14
6	67.00	93.76	84.46
7	66.00	91.89	81.91
8	67.00	94.35	83.86
9	69.00	93.76	84.25
10	67.00	93.76	83.46

Table 3. Experimental results of feature dimension of Sobel gradient magnitude information

4.5 HSV color space verification

During the experiments, HSV color space was applied to extract WLD histogram features of photographic images and photorealistic computer graphics. To verify the validity of HSV color space, WLD histogram features of the two kinds of images were extracted from RGB color space and used to detect the images. The experimental results are shown in Table 4.

As shown in Table 4, the detection rate of WLD histogram features extracted from HSV color space was up to 95.44% (about 5% higher than that of similar features extracted from RGB color space), which indicated that the features extracted from HSV color space were more suitable for the identification of photographic images and computer

Color space	RGB algorithm	HSV algorithm
TP (%)	85.48	94.98
TN (%)	93.31	95.79
Accuracy (%)	89.78	95.43
feature dimension	60	60

Table 4. Experimental results with different color space

generated images.

5. Conclusion

In view of the problems in blind identification algorithms for photorealistic computer graphics, such as high feature dimensions and unsatisfactory detection rate, this study proposed a new blind identification algorithm for photorealistic computer graphics based on Weber local features. Firstly, RGB images in the image library were transformed to HSV images; after separation, three single-channel images (H, S and V) were obtained. Then, Weber local features of each single-channel image were extracted, including the histogram features of differential excitation information, Sobel gradient direction information and Sobel gradient magnitude information; in total, 60 dimensional classification features were obtained. At last, SVM classifiers were used for training and classification, thus to implement blind identification of photorealistic computer graphics. Compared with other algorithms, the algorithm in this study has a promising development prospect with its higher detection rate (95.43%) and lower dimension of classification features.

6. Acknowledgement

Project of Natural Science Foundation of Sichuan Provincial Department of Education (16ZB0078).

References

[1] Kang, X B., Wei, S M (2013). Identifying Tampered Regions Using Singular Value Decomposition in Digital Image Forensics, *In:* International Conference on Computer Science & Software Engineering, 4400-18.

[2] Chervyakov, N I., Lyakhov, P A., Babenko, M G. (2014). Digital filtering of images in a residue number system using finite-field wavelets. *Automatic Control & Computer Sciences*, 48 (3) 180-189.

[3] Redi, J. A., Taktak, W., Dugelay, J L. (2011). Digital image forensics: a booklet for beginners. *Multimedia Tools & Applications,* 51 (1) 133-162.

[4] Cao, H ., Kot, A C. (2009). Accurate Detection of Demosaicing Regularity for Digital Image Forensics. *Information Forensics & Security IEEE Transactions on,* 4 (4) 899-910.

[5] Li, C.T., Li, Y (2012). Color-Decoupled Photo Response Non-Uniformity for Digital Image Forensics. *IEEE Transactions on Circuits & Systems for Video Technology*, 22 (2) 260-271.

[6] Gloe, T., Borowka, K., Winkler, A (2010). Efficient estimation and large-scale evaluation of lateral chromatic aberration for digital image forensics. *Proceedings of SPIE - The International Society for Optical Engineering,* 7541 (1) 754107-754107-13.

[7] Liu, ZL., Li, XH., Zhao, YQ (2011). Passive Detection of Copy-paste Tampering for Digital Image Forensics. *In:* International Conference on Intelligent Computation Technology and Automation, 649-652.

[8] Ho. J S., Au, O C., Zhou, J, (2010). Inter-channel demosaicking traces for digital image forensics. *In*: IEEE International Conference on Multimedia & Expo. IEEE, 1475-1480.

[9] Swaminatha, A., Wu, M., Liu, K J R (2008). Digital image forensics via intrinsic fingerprints. *IEEE Transactions on Information Forensics & Security,* 3 (1) 101-117.

[10] Korus, PHuang, J (2016). Improved Tampering Localization in Digital Image Forensics Based on Maximal Entropy Random Walk. *IEEE Signal Processing Letters*, 23 (1) 169-173.

[11] Qu, Z H., Luo, W Q., Huang, J W (2014). A framework for identifying shifted double JPEG compression artifacts with application to non-intrusive digital image forensics. Science in China, 57 (2) 1-18.

[12] Chen, J ., Shan, SG., He, C (2010). WLD: a robust local image descriptor. *Pattern Analysis & Machine Intelligence IEEE Transactions on*, 32 (9) 1705-20.

[13] Anamandra, S H., Chandrasekaran, V (2013). CHILD: A robust Computationally-Efficient Histogram-based Image Local Descriptor. Computer Vision, Pattern Recognition, Image Processing and Graphics. IEEE, 1 - 5.

[14] Gragnaniello, D., Poggi, G., Sansone, C.(2013). Fingerprint Liveness Detection based on Weber Local Image Descriptor, *In:* Biometric Measurements and Systems for Security and Medical Applications (BIOMS), 2013 IEEE Workshop on. IEEE, 46 - 50.

[15] Wang, X., Jin, C., Liu, W (2013). Feature fusion of HOG and WLD for facial expression recognition. *In:* International Symposium on System Integration, 227-232.

[16] Walia, E., Suneja, A . Digital Image WatermarkingTechnique Based on Dense Descriptor. High Performance Architecture and Grid Computing. Springer Berlin Heidelberg, 612-616.

[17] Ullah, I., Hussain, M., Muhammad, M (2012). Gender

Recognition From Face Images With Spatial WLD Descriptor. *In*: IEEE International Conference on Systems, Signals and Image Processing, 417 – 420.

[18] Han, X H., Chen, Y W., Xu, G (2014). High-Order Statistics of Weber Local Descriptors for Image Representation. *Cybernetics IEEE Transactions on*, 45 (6) 1180-1193.

[19] Zhao, J., Liu, M (2008). A Color HSV Image Edge Detection Method Based on Gradient Extreme Value, *In*: Proceedings of the 2008 Second International Symposiumon Intelligent Information Technology Application - Volume03. IEEE Computer Society, 381-384.

[20] Zhao, G., Wang, S., Wang, T(2008). HSV Color Space and Face Detection Based Objectionable Image Detecting, *In*: Second International Conference on Future Generation Communication and Networking Symposia. IEEE Computer Society, 107-110, .

[21] Liu, C., Lu, X ., Ji, S (2014). A fog level detection method based on image HSV color histogram, *In*: International Conference on Progress in Informatics and Computing. IEEE, 373-377,.

[22] Chang, C C Lin, C J (2011). LIBSVM: A library for support vector machines, *ACM Transactions on Intelligent Systems & Technology,* 2 (3) 389-396.